Infrared Characterization of the Icosahedral Shell Closing in $Cl^-\cdot H_2O\cdot Ar_n$ ($1 \le n \le 13$) Clusters

S. A. Corcelli, J. A. Kelley, J. C. Tully, and M. A. Johnson*

Sterling Chemistry Laboratory, Yale University, P.O. Box 208107, New Haven, Connecticut 06520

Received: October 25, 2001; In Final Form: February 15, 2002

The mid-infrared predissociation spectra of $Cl^-\cdot H_2O\cdot Ar_n$ clusters are dominated by an intense band that is due to excitation of the ionic H-bonded OH stretching vibration. The shape of this band is found to be quite sensitive to the number of attached argon atoms, becoming incrementally narrower until $n = 11$, the size at which a strong "magic number" appears in the cluster intensity profile. This observation is consistent with the formation of a capped icosahedral structure where the water molecule replaces one argon atom in the closed shell $Cl^-\cdot Ar_{12}$ structure. This conjecture is supported by a theoretical study of the $Cl^-\cdot H_2O\cdot Ar_n$ structures using a simulated annealing procedure. These calculations find only one isomeric form for $n = 11$ but identify several distinct local minima for $n \neq 11$. We recover the qualitative features of the band envelopes by calculating the electrostatic effects of the various isomeric forms on the potential energy surface describing the motion of a hydrogen atom toward the chloride ion.

Introduction

We have recently carried out a series of infrared studies[1−4] on the $X^-\cdot H_2O$ (X = halide) complexes in order to establish the structures and spectroscopic signatures of the halide monohydrates. The asymmetric structure, in which one hydrogen is attached to the ion while the other remains free, results in a characteristic pattern where the OH engaged in the ionic hydrogen bond (IHB) dominates the mid-infrared spectrum.[5] The IHB fundamentals are generally shifted hundreds of wavenumbers below the centroid of the two bands in bare water in a manner correlated with the binding energies of the complexes. These patterns were anticipated by ab initio calculations,[6−15] leading Thompson and Hynes[14] to consider the qualitative origins of the shifts. They concluded that, although most of the shift arises from electrostatics,[16] about 40% of the band displacement in $Cl^-\cdot H_2O$ (~570 cm^{-1}) can be traced to charge-transfer into the OH antibonding orbital. The latter effect evolves into the strongly distorted potential curve governing the OH stretch in the neighborhood of the intracluster proton-transfer reaction:

$$Cl^- + H_2O \rightarrow OH^- + HCl. \qquad (1)$$

This system, therefore, provides a spectroscopically accessible reaction coordinate, and here we explore how the shape of this potential surface responds to stepwise addition of argon atoms in a vibrational study of the $Cl^-\cdot H_2O\cdot Ar_n$ clusters.

The present paper follows two previous reports[1,17] in which we have established the band assignments of the chloride−water complex using argon predissociation spectroscopy:[4]

$$Cl^-\cdot H_2O\cdot Ar_n + h\nu \rightarrow Cl^-\cdot H_2O + nAr \qquad (2)$$

for $n \le 5$. A typical spectrum is reproduced in Figure 1 illustrating the locations of the various bands. The IHB band dominates the spectrum at 3140 cm^{-1}, with weaker bands assigned to the IHB in combination with the ion−molecule (IM) stretch, the $2 \leftarrow 0$ overtone of the intramolecular bending vibration (B), and the free OH stretch (F) at 3695 cm^{-1}. Although this basic pattern was found to be insensitive to the number of argon atoms, we noted in a previous paper[17] that the widths of the bands depended strongly on the vibrational character of the excited mode. Those bands derived from IHB excitation (i.e., the IHB fundamental and the ion−water stretching combination band) were significantly broader than those associated primarily with intramolecular motion (i.e., the bend overtone and the free OH stretch). In this paper, we report the evolution of the IHB band envelopes in the $Cl^-\cdot H_2O\cdot Ar_n$ ($1 \le n \le 13$) clusters and interpret the size-dependence of these shapes by considering how different arrangements of argon atoms distort the proton-transfer reaction coordinate in the $Cl^-\cdot H_2O$ entrance channel complex.

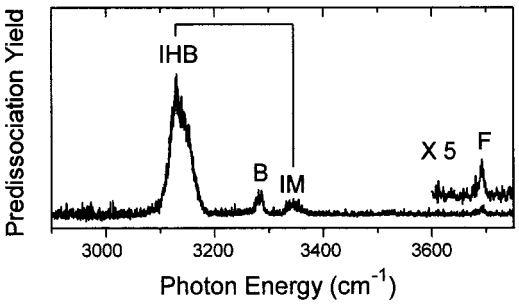

Figure 1. Previously reported (ref 1) vibrational predissociation spectrum of $Cl^-\cdot H_2O\cdot Ar_3$. The bands are assigned as an ionic H-bonded OH stretch (IHB), the first overtone of the water bend (B), and the free OH stretch (F). The brackets indicate a combination band arising from the IHB and the low-frequency ion−molecule (IM) stretching motion.

Experimental Section

The $Cl^-\cdot H_2O\cdot Ar_n$ clusters central to this study were generated by condensing water molecules onto $Cl^-\cdot Ar_n$ clusters:

$$Cl^-\cdot Ar_n + H_2O \rightarrow Cl^-\cdot H_2O\cdot Ar_m + (n - m)Ar \qquad (3)$$

* To whom correspondence should be addressed.

10.1021/jp013956k CCC: $22.00
Published on Web 04/11/2002

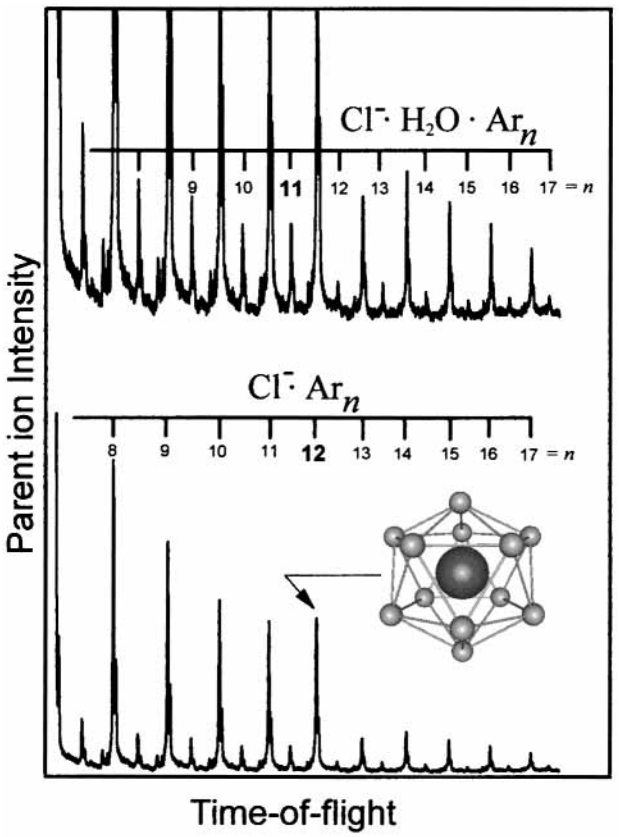

Figure 2. Time-of-flight mass spectra of the $Cl^-\cdot Ar_n$ and $Cl^-\cdot H_2O\cdot Ar_n$ clusters. The lower trace displays a magic number in the $Cl^-\cdot Ar_n$ progression at $n = 12$, corresponding to the icosahedral arrangement (inset) reported by Neumark and co-workers (ref 22). The upper trace shows a magnified view of the interloping $Cl^-\cdot H_2O\cdot Ar_n$ peaks, which display a magic number at $n = 11$.

The precursor $Cl^-\cdot Ar_n$ clusters were formed by introduction of $CHCl_3$ vapor just outside the orifice of a pulsed supersonic jet of pure argon, ionized by a coaxial, counterpropagating electron beam. H_2O vapor was then introduced as background gas in the source chamber (5×10^{-5} Torr), which was entrained[18] or aspirated into the supersonic flow. Infrared spectra were obtained with the Yale tandem time-of-flight photofragmentation spectrometer described previously.[19] Infrared radiation was generated using a Nd:YAG pumped KTP/KTA optical parametric oscillator/amplifier (LaserVision). The reported spectra result from the average of typically 30 individual scans and are normalized for changes in the laser output energy over the scan. The beam path was purged with dry N_2 to avoid absorption by ambient water vapor.

Results and Discussion

A. Cluster Intensity Distributions and Calculated Shell Structures. Figure 2 presents the parent ion intensity distributions generated by the entrainment ion source. The lower trace highlights the precursor $Cl^-\cdot Ar_n$ clusters, which display a strong intensity discontinuity at $n = 12$. Such special behavior at $n = 12$ has been reported to occur in other $X^-\cdot RG_n$ (X = halide, RG = rare gas) systems and analyzed in terms of an icosahedral shell closing such as that depicted in the inset in Figure 2. Examples are $O^-\cdot Ar_n$,[20] $I^-\cdot Xe_n$,[21] and $Cl^-\cdot Ar_n$,[22,23] which were characterized by negative ion photoelectron spectroscopy. In the $I^-\cdot Xe_n$ system, Becker et al.[21] were able to deduce that the binding energy of the 13th Xe is about a factor of 2 less than that of the 12th, which is readily understandable because the 13th particle is forced to reside outside the first solvation shell.

More interesting in the present context, however, is the intensity distribution of the mixed $Cl^-\cdot H_2O\cdot Ar_n$ clusters, which appear as the weaker interlopers between the strong $Cl^-\cdot Ar_n$ peaks in Figure 2. Inspection of these smaller peaks, highlighted in the expanded spectrum at the top of Figure 2, indicates that there is a similarly strong break-off intensity, but this time at $n = 11$. This suggests that a water molecule has replaced one of the argon atoms in the icosahedral arrangement.

To test the plausibility of a "substituted" icosahedron structure for the $Cl^-\cdot H_2O\cdot Ar_{11}$ cluster, we have carried out a series of calculations using a simulated annealing Monte Carlo (MC) method to obtain structures for the mixed $Cl^-\cdot H_2O\cdot Ar_n$ clusters. The overall strategy is similar to that recently reported by Neumark and co-workers[22,23] for $X^-\cdot Ar_n$ (X = Cl, Br, and I) clusters. In our approach, the potential energy, U, is written as a sum of pair interactions between species in the cluster:

$$U = U_{W-Cl^-} + U_{Ar-W} + U_{Ar-Cl^-} + U_{Ar-Ar} \qquad (4)$$

The explicit form and characteristics of these pairwise interactions have been reported elsewhere and for brevity will not be repeated here. Parameters for the U_{W-Cl^-} interaction potential energy of Dorsett, Watts, and Xantheas[8] were determined by fitting ab initio (MP4/aug-cc-pVTZ) $Cl^-\cdot H_2O$ minimum energies and geometries as a function of Cl^-—O separation. In this work, we have modified their chloride—water potential in that we held the water molecule rigid. This was accomplished by constraining the distorted internal geometry of the water molecule to that found in the minimum energy $Cl^-\cdot H_2O$ structure. For small excursions from the equilibrium Cl^-—O distance, fixing the H_2O internal geometry has negligible effect on the relative orientation of the water molecule with respect to the chloride ion. The AW2 potential developed by Cohen and Saykally[24] was used for the interaction between water and Ar, U_{Ar-W}. The AW2 potential was developed by fitting 12 parameters to 37 vibration—rotation—tunneling (VRT) transitions observed for the $Ar\cdot H_2O$ and $Ar\cdot D_2O$ complexes. For the interaction of Ar with the chloride ion, U_{Ar-Cl^-}, the potential developed by Lenzer et al.[25] was used. In their work, potentials for both $Ar-Cl^-$ and several electronic states of neutral Ar·Cl were obtained by analyzing zero-electron kinetic energy (ZEKE) spectra of $Ar\cdot Cl^-$. Finally, the interaction between a pair of Ar atoms, U_{Ar-Ar}, was modeled using the Hartree—Fock dispersion potential (HFD-B2) of Aziz and Slaman.[26] Parameters for this potential were determined by integrating spectroscopic, scattering, and bulk data.

Structures for the $Cl^-\cdot H_2O\cdot Ar_n$ clusters were obtained using a simulated annealing MC method. The initial cluster geometry was taken to be the $Cl^-\cdot H_2O$ core ion at its minimum energy configuration with n Ar atoms randomly placed in a sphere of radius 5.5 Å, centered about the chloride ion. No $Ar-H_2O$, $Ar-Cl^-$, or Ar—Ar distance less than 3.6 Å was allowed to ensure that the cluster begins in an attractive region of the potential. An initial rapid quench was performed to avoid evaporation of Ar atoms. The rapid quench typically involved 10^4 attempted MC moves of the water and Ar atoms with an exceedingly small temperature of 0.005 K. Following the quench, MC moves were attempted with an initial temperature of 50 K. After every 5000 attempted MC moves, the temperature was decreased by 0.5 K down to a temperature of 1 K. The temperature was then divided by two every 10000 attempted MC steps until a final temperature of less than 10^{-6} K was achieved. The total number of MC steps attempted in the procedure was over 6×10^6. For each $Cl^-\cdot H_2O\cdot Ar_n$ cluster studied, the simulated annealing procedure was repeated for 100 different initial random cluster configura-

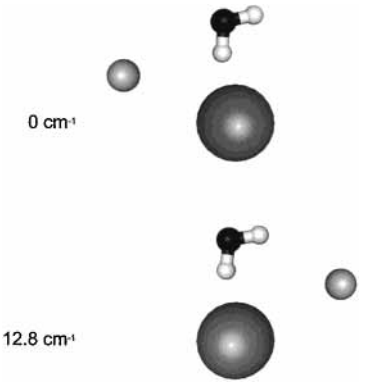

Figure 3. Structures and relative energies from a simulated annealing calculation of the $Cl^-\cdot H_2O\cdot Ar$ complex. The large gray sphere is Cl^-, and the smaller one is Ar.

tions. This was done to enhance the possibility of finding a variety of energetically low lying isomers (local minima).

Figures 3 and 4 display the structures of the low lying isomers recovered in our simulated annealing procedure for $Cl^-\cdot H_2O\cdot Ar_n$ (n = 1, 10, 11, and 12). All 100 random initial cluster configurations with n = 11 yielded the same substituted icosahedral structure shown in Figure 4b; no additional local minima were found. In contrast, for n = 1, two different isomers were found with all of the atoms lying approximately in a plane but with the Ar occupying a site adjacent either to the IHB or to the free OH as depicted in Figure 3. These two isomers differ in energy by only 12.8 cm^{-1}. For n = 10, three different classes of isomers were found with an example of each class shown in Figure 4a. Interestingly, these are derived from the icosahedral motif found for the n = 11 cluster, where one of the Ar atoms is removed to form a "hole". In the lowest energy class, the hole is located in the ring of Ar atoms encircling the water molecule. The clusters have slightly different energies (within about 1 cm^{-1}) depending on which Ar atom is removed from the ring. The next higher energy class has the hole in the second ring of Ar atoms with respect to the water molecule. These isomers are calculated to lie about 13 cm^{-1} higher in energy than the minimum energy n = 10 cluster. The highest energy isomer (16.0 cm^{-1} above the minimum) is shown on the right side of Figure 4a, where the hole appears at the site of the capping argon atom transverse to the water molecule in the icosahedral motif.

The two lowest energy n = 12 isomers are shown in Figure 4c, where the additional Ar atom begins to form a second solvation shell. These low energy n = 12 isomers differ in energy by 13.6 cm^{-1} and are reminiscent of the n = 1 forms in that the Ar binds to the O atom or the free OH. A somewhat higher energy isomer was also recovered in which the extra argon atom inserts into the first solvation shell, forming a ring of six argon atoms around the water molecule (as opposed to the five membered rings which surround the water in the icosahedron-based arrangements). This isomer is shown on the right side of Figure 4c and lies 47.4 cm^{-1} above the minimum energy arrangement.

For $2 \le n \le 9$ [not shown in Figures 3 and 4], there tend to be many low lying $Cl^-\cdot H_2O\cdot Ar_n$ isomers within 50 cm^{-1} of the minimum energy structure. This is not surprising because, for example, in the n = 6 cluster, there are five holes which can be arranged in 11!/6! = 55440 different ways, many of which will be similar in energy. Obviously, this scheme counts arrangements as distinct isomers, when in reality, they may not be separated by barriers.

B. Predissociation Spectra for $Cl^-\cdot H_2O\cdot Ar_n$, $1 \le n \le 13$. Figure 5 presents an overview of the predissociation spectra:

$$Cl^-\cdot H_2O\cdot Ar_n + h\nu \rightarrow Cl^-\cdot H_2O\cdot Ar_m + (n-m)Ar \quad (5)$$

For the larger clusters (i.e., n > 6), photoexcitation at ~3150 cm^{-1} results in a typical statistical evaporation of argon atoms

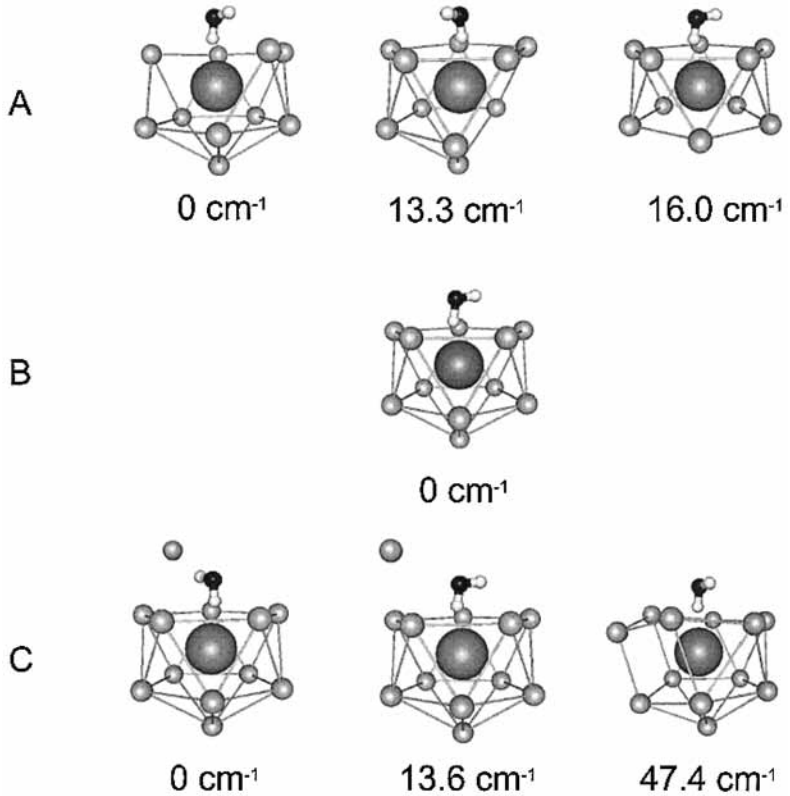

Figure 4. Structures and relative energies from simulated annealing of $Cl^-\cdot H_2O\cdot Ar_n$ [n = 10 (A), 11 (B), and 12 (C)]. The energy values pertain to the relative stability of isomers with the same value of n.

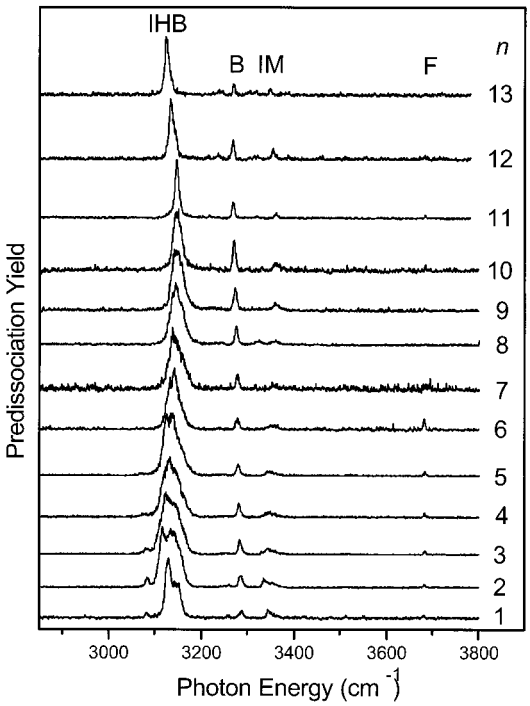

Figure 5. Vibrational predissociation spectra of $Cl^-\cdot H_2O\cdot Ar_n$ ($n = 1-13$). IHB = ionic H-bonded OH stretch, B = intramolecular H_2O bending overtone, F = free OH stretch, and IM = IHB + ion−molecule stretch combination band. Each spectrum is normalized to the most intense feature in the scan.

with a mean loss of about five atoms. Thus, for $n < 5$, the entire spectrum can be recorded by monitoring the $Cl^-\cdot H_2O$ photoproduct as it is the dominant fragment over the entire range. The situation is more complicated in the higher clusters, however, because the mean argon loss increases with increasing photon energy across the scan. Because we are most interested in the evolution of the IHB feature with argon solvation, the spectra of the larger clusters in Figure 5 were taken by gating the fragment mass spectrometer on the most intense product ion generated by excitation at the peak of the IHB band (typically evaporation of five atoms). This suppresses the free OH region, as absorption at $\sim$3700 cm^{-1} results in a mean loss of six argon atoms.

Note that the basic pattern is quite insensitive to the extent of argon solvation, with the dominant band assigned to the IHB fundamental, flanked on the high energy side by the bend overtone (B) and ion−molecule stretching combination band (IM). The free OH stretching band (F) is essentially unshifted upon solvation, whereas the bend overtone shifts very slowly toward lower energy (-20 cm^{-1} by $n = 13$). Because the IM band follows the IHB stretching position, the shift in the bend overtone has the effect of opening the gap between the B and IM bands with increasing cluster size. There is a small peak about 50 cm^{-1} below the IHB band in the $n = 1$ spectrum, which is gradually suppressed upon addition of argon atoms such that it disappears by $n = 5$ or so. In light of the fact this shift is very similar to the hot band displacement observed in the bare $Cl^-\cdot Ar$ cluster (53 cm^{-1}) by Neumark and co-workers,[25] we assign this feature to a hot band transition arising from analogous Ar motion. This assignment is consistent with the suppression of the band because the internal energy can be accommodated by increasingly soft modes available in the larger clusters.

Although the envelopes of the free OH and bend overtone bands are quite narrow, the IHB and IM bands are much broader.

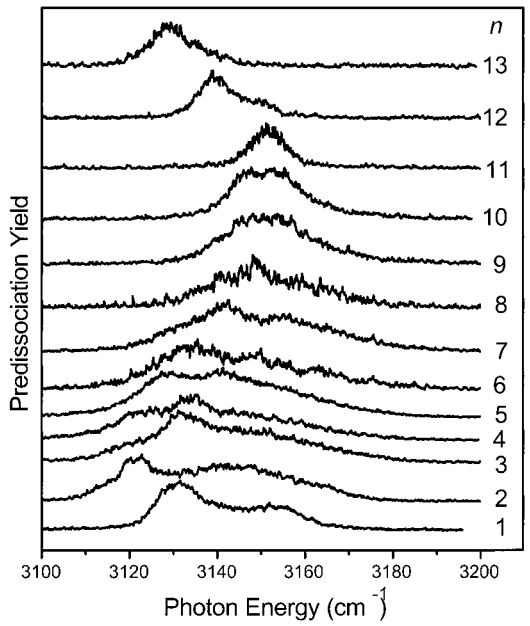

Figure 6. Vibrational predissociation spectra of $Cl^-\cdot H_2O\cdot Ar_n$ ($n = 1-13$) with an expanded view of the ionic H-bonded (IHB) OH stretch region. Each spectrum is normalized to the most intense feature in the scan.

The IHB band indeed displays some distinct multiplet structure, especially for the first few argon atoms. We present an expanded view of the IHB region in Figure 6. The most striking aspect of this progression is the reduction of the bandwidths with increasing argon solvation, leading to a minimum at $n = 11$, the cluster size associated with the shell closing as discussed in the previous section. Interestingly, the band generally shifts toward higher energy up until $n = 11$ and then promptly falls back toward lower energy upon addition of the 12th argon atom.

We have observed a similar trend, where the IHB broadens with the number of attached argon atoms in our earlier studies of the $I^-\cdot ROH\cdot Ar_n$, (R-methyl, ethyl, and isopropyl) clusters.[27] In that work, the spectra display a series of resolved peaks, where a new peak appears on the low energy side of the IHB band with each additional argon. Most importantly, peaks present in the smaller clusters persist in the spectra of higher clusters with a small shift toward higher energy. This has the effect of broadening the IHB bands to sizes in the range of $n = 5$ before the envelopes begin to narrow. Unfortunately, we did not follow the behavior of the alcohols out to sufficiently high n to establish whether the bandwidths pass through a minimum such as that observed here.

The multiplets observed in the $I^-\cdot ROH\cdot Ar_n$ spectra were interpreted to reflect the presence of isomers in which some of the Ar binding sites lead to a red shift in the IHB while other sites lead to a smaller blue shift.[27] Thus, the location of a peak in the spectrum encodes the number of argon atoms in a particular site. In this context, the breadth of the IHB band narrows when the sites become saturated, reducing the number of spectroscopically distinct arrangements.

The fact that the IHB band in $Cl^-\cdot H_2O$ is narrowest at the (capped icosahedral) closed shell structure leads us to suspect that the larger widths in other cluster sizes may arise from the different isomeric forms yielding different shifts, just as in the $I^-\cdot ROH\cdot Ar_n$ case. On a qualitative level, the first few argon atoms clearly lead to sequential red shifts of the IHB band, indicating that the proximity of an argon atom [see Figure 3]

tends to slightly soften the OH stretch in an additive manner. The multiplet structure can then be readily explained as being due to very cold members of the ensemble, which have the argon bound next to the water, together with warmer clusters where the argon is detached from the water but remains bound to the ion. In an icosahedral arrangement, there are five atoms surrounding a vertex, which suggests that we should find a maximum red shift at $n = 5$. Higher energy transitions would then arise from other isomers containing sequentially larger numbers of argon atoms distant from the water molecule in the evaporative ensemble.[28] This expectation is qualitatively in line with the trends observed in Figure 6, where the maximum red shift is displayed in the size range of $n = 4-6$ before the bands narrow and evolve toward higher energy. This agreement motivated us to develop a quantitative model for the shifts discussed in detail in the next section.

C. Calculation of Solvent Effects on the IHB Band Position. In an earlier theoretical study of how argon atoms effect the $Cl^-\cdot H_2O$ vibrational spectrum, Iwata and co-workers[29] carried out ab initio calculations on the entire $Cl^-\cdot H_2O\cdot Ar_n$ cluster and extracted harmonic vibrational frequencies. This method dramatically overestimated the argon shifts (-50 cm^{-1}/Ar) compared to those observed experimentally ($\sim\pm 10$ cm^{-1}/Ar), and we have therefore adopted an alternative strategy. In our approach, we quantify the effect of a specific argon arrangement on the OH_{IHB} stretch frequency by considering the electrostatic solvation of the $Cl^-\cdot H_2O$ core ion along the IHB bond displacement. This approach takes advantage of the fact that the $Cl^-\cdot H_2O$ system is sufficiently small that the coordinate-dependence of the electronic structure can be accurately described through high level ab initio calculations. To establish the magnitude of the effects, we treat the special case where we freeze the argon atoms at their minimum energy positions and explore the argon position dependence of the IHB $\nu = 0-1$ energy gap. This ignores the role of high amplitude motion of both the water molecule and the argon atoms in their zero-point vibrational levels and would only be expected to provide a quantitative description in the limit of high barriers separating the isomeric forms. In the $n = 1$ case, this barrier is calculated to be modest (about 30 cm^{-1} compared to the energy difference between isomers, 12.8 cm^{-1}), so the small clusters are likely to require explicit treatment of the soft modes to simulate the observed spectra. In light of the present situation in the literature,[29] however, it is nonetheless informative to quantify the magnitude of the argon shifts in the static case.

To begin, we optimized the $Cl^-\cdot H_2O$ geometry at the MP2 level of theory with an augmented correlation-consistent, polarized valence basis set (aug-cc-pVTZ).[30,31] The optimized structure is very close to that published by Xantheas using MP4/aug-cc-pVTZ.[32] Starting from the optimized $Cl^-\cdot H_2O$ structure, the potential energy of the OH_{IHB} stretch local mode was mapped by performing single-point energy calculations in which the OH bond was incrementally displaced from its equilibrium position in the direction of its bond axis, with the distance between the chloride ion and the water oxygen atom held fixed at 3.1 Å. Figure 7 displays the resulting potential energy profile, $V(x)$. The characteristic distortion of the potential energy curve which is due to the proton-transfer reaction, eq 1, is clearly evident for large displacements in the direction of the chloride ion ($x > 0$). Also shown in Figure 7 is a fit of the potential well to a Morse oscillator over a range of OH displacements from $x = -0.2$ to $+0.4$ Å, as well as the energies of the resulting $\nu = 0$, 1, and 2 vibrational levels. Although these levels explore

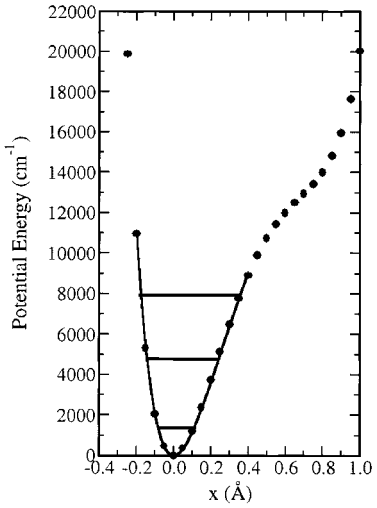

Figure 7. (Filled circles) ab initio (MP2 level of theory with an aug-cc-pVTZ basis set) potential energy function for displacement, x, of the hydrogen bonded to the chloride in the direction along the OH bond axis. (Line) Morse oscillator fit to the ab initio data over a range of displacements $x = -0.2 \le x \le 0.4$. Also shown are the $\nu = 0-2$ vibrational energy levels of the Morse oscillator.

displacements below the "shelf" in the potential, note that there is nonetheless significant, coordinate-dependent charge-transfer character in the electronic wave function.[14] It is the latter effect which gives rise to selective perturbation of the $Cl^-\cdot H_2O$ core ion along the IHB coordinate.

Having characterized the OH_{IHB} stretch in the bare $Cl^-\cdot H_2O$ complex, we can now consider how a given configuration of n Ar atoms shifts its IHB vibrational frequency. In our model, the $Cl^-\cdot H_2O\cdot Ar_n$ cluster was viewed as a collection of partial charges and induced point dipoles. Partial charges were centered on the Cl^- ion and on each atom in the water molecule, whereas the Ar atoms were assumed to be neutral. Each of the species in the cluster was assigned a polarizability, and induced dipoles were placed on the Cl^- ion, each of the Ar atoms, and on the O atom of the water molecule. The polarizabilities assigned were 1.64 Å^3 for Ar,[33,34] 4.17 Å^3 for the chloride ion (the result of an MP4/aug-cc-pVTZ calculation), and 1.45 Å^3 for water[35] (the small anisotropy in the water polarizability was ignored).

Partial charges for the $Cl^-\cdot H_2O$ complex were obtained by analyzing the MP2/aug-cc-pVTZ electron density, ρ. Of course, there is no unique method for assigning partial charges to atomic centers based on ρ, so in this work, we considered two commonly used approaches, Mulliken charges and atoms-in-molecules (AIM) charges. Mulliken charges are assigned by considering the electron population in the atomic-centered basis function, whereas the AIM method seeks to define atoms within the system by locating surfaces of vanishing electron density flux, $\nabla\rho = 0$.[36] In the latter case, charges are determined by simply integrating ρ over the region of space assigned to each atom. Mulliken charges are known to be more basis set dependent than AIM charges.

The induced dipole moment, $\boldsymbol{p}_i$, for each species in the $Cl^-\cdot H_2O\cdot Ar_n$ cluster is proportional to the electric field at the location of the induced dipole, $\boldsymbol{E}_i$

$$\mathbf{p}_i = \alpha_i \mathbf{E}_i, \tag{6}$$

where α_i is the scalar polarizability of species i. The electric field at the position of the induced dipole moment of species i

results from charges in the system not associated with species *i* and from the other induced dipole moments in the system

$$\mathbf{E}_i = \mathbf{E}_i^{\,0} + \sum_{j=1,j\neq i}^{N} \mathbf{T}_{ij}\mathbf{p}_j = \sum_{j=1,j\neq i}^{N}\sum_{k=1}^{M_j} \frac{1}{4\pi\epsilon_0}\frac{q_k\mathbf{r}_{ik}}{r_{ik}^{\,3}} + \sum_{j=1,j\neq i}^{N} \mathbf{T}_{ij}\mathbf{p}_j \tag{7}$$

where N is the number of induced dipole moments in the $Cl^-\cdot H_2O\cdot Ar_n$ cluster ($N = n + 2$), M_j is the number of charges associated with species j ($M_j = 1$ for Ar and Cl^- and $M_j = 3$ for water), ϵ_0 is the vacuum permittivity, and $\boldsymbol{r}_{ik}$ is the vector from induced dipole i to charge q_k. $\boldsymbol{T}_{ij}$ represents the traceless dipole tensor:

$$\mathbf{T}_{ij} = \frac{1}{4\pi\epsilon_0}\frac{1}{r_{ij}^{\,3}}\left[\frac{3\mathbf{r}_{ij}\mathbf{r}_{ij}}{r_{ij}^{\,2}} - 1\right] \tag{8}$$

where $\boldsymbol{r}_{ij}$ is the vector from induced dipole i to induced dipole j. The induced dipole moments were determined iteratively by making an initial guess for each $\boldsymbol{p}_i$, calculating the electric field, $\boldsymbol{E}_i$, using eq 7, and substituting into the right-hand side of eq 6 to obtain a refined value of $\boldsymbol{p}_i$. This process was repeated until self-consistency was achieved.

The total electrostatic energy of a collection of charges and induced dipoles is given by

$$U = U_{qq} + U_{qp} + U_{pp} + U_{\text{self}} \tag{9}$$

U_{qq} is the Coulombic energy of the charges

$$U_{qq} = \frac{1}{2}\sum_{i=1}^{N_q}\sum_{j=1,j\neq i}^{N_q} \frac{1}{4\pi\epsilon_0}\frac{q_iq_j}{r_{ij}} \tag{10}$$

with N_q denoting the number of charges in the system (four in this case) and r_{ij} representing the distance between charges i and j. U_{qp} is the interaction energy between the charges and induced dipoles

$$U_{qp} = -\sum_{i=1}^{N}\mathbf{p}_i\cdot\mathbf{E}_i^{\,0} \tag{11}$$

where $\boldsymbol{E}_i^{\,0}$ is the electric field from the charges in the system not associated with species i as defined in eq 7. U_{pp} is the interaction energy of the induced dipoles

$$U_{pp} = -\frac{1}{2}\sum_{i=1}^{N}\sum_{j=1,j\neq i}^{N}\mathbf{p}_i\cdot\mathbf{T}_{ij}\cdot\mathbf{p}_j \tag{12}$$

and U_{self} is the energy needed to create the induced dipoles

$$U_{\text{self}} = \sum_{i=1}^{N}\frac{\mathbf{p}_i\cdot\mathbf{p}_i}{2\alpha_i} \tag{13}$$

The electrostatic solvation energy for a given fixed configuration of a $Cl^-\cdot H_2O\cdot Ar_n$ cluster, ΔU, is simply the difference between the electrostatic energy of the entire cluster, U_n, and that of the $Cl^-\cdot H_2O$ core, U_0

$$\Delta U = U_n - U_0 \tag{14}$$

For a given isomeric form of the $Cl^-\cdot H_2O\cdot Ar_n$ cluster, the frequency of the OH_{IHB} stretch was determined by calculating the solvation energy, $\Delta U(x)$, over a range of OH displacements from $x = -0.2$ to $+0.4$ Å and adding it to the OH stretch potential energy curve $V(x)$. At each OH displacement, Mulliken and AIM partial charges for the $Cl^-\cdot H_2O$ complex were obtained from a separate MP2/aug-cc-pVTZ calculation, and ΔU was computed using eq 14. The corrected potential, $V'(x) = V(x) + \Delta U(x)$, was fit to a Morse form so that the vibrational energy levels could be recovered analytically. The shift in the OH_{IHB} fundamental frequency was then estimated from the $\nu = 0 \rightarrow 1$ energy spacing relative to that in the unperturbed Morse oscillator.

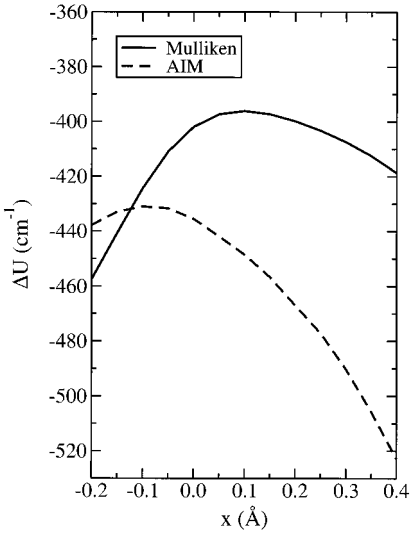

Figure 8. Solvation energy, ΔU, for the lowest energy $Cl^-\cdot H_2O\cdot Ar$ isomer as a function of the displacement of the ionic H-bonded hydrogen using Mulliken (solid) and AIM (dotted) point charges.

Figure 8 displays the coordinate-dependent solvation energy, $\Delta U(x)$, for the lowest energy $Cl^-\cdot H_2O\cdot Ar$ isomer depicted in Figure 3. The qualitative difference between the solvation energies computed using Mulliken and AIM charges is immediately obvious. In the Mulliken charge scheme, shorter values of the OH stretch are preferentially solvated, opposite to the trend predicted using the AIM charge scheme. These corrected potentials give shifts in the OH_{IHB} stretch frequency of -10.6 cm^{-1} for the AIM charges and -3.1 cm^{-1} for the Mulliken charges. Analysis of the higher energy $Cl^-\cdot H_2O\cdot Ar$ isomer [lower trace in Figure 3b] yields a $+4.3$ cm^{-1} shift for the AIM charges and a $+5.0$ cm^{-1} shift for the Mulliken charges. Thus, for the $Cl^-\cdot H_2O\cdot Ar$ cluster, our calculations predict two peaks in the OH_{IHB} stretch spectrum separated by 8.1 cm^{-1} for Mulliken charges and 14.9 cm^{-1} for the AIM charges. The experimental $Cl^-\cdot H_2O\cdot Ar$ spectrum [bottom trace in Figure 6] shows a distinct doublet structure with a peak separation of about 20 cm^{-1}, in fair agreement with the AIM calculation.

Figure 9 compares the stick spectra for the expected OH_{IHB} fundamentals arising from the $Cl^-\cdot H_2O\cdot Ar_n$ ($n = 0-2$) isomers obtained in our simulated annealing calculations. The two panels indicate the patterns calculated using Mulliken (left) and AIM (right) charges. Qualitatively, the AIM charges recover the experimental trends, whereas the Mulliken charges do not. Most notably, the calculated spectrum for the $n = 2$ cluster using AIM charges correctly predicts a new transition to the red of both $n = 1$ peaks. This peak is spaced 15.2 cm^{-1} below the centroid of a closely spaced doublet. The experimental $Cl^-\cdot H_2O\cdot Ar_2$ spectrum contains two peaks separated by roughly 25 cm^{-1}. Interestingly, in the experiment, the lowest energy peak is noticeably narrower than the structure toward higher energy [$n = 2$ spectrum in Figure 6]. Given the internal energy contained in the $Cl^-\cdot H_2O\cdot Ar_n$ cluster ensemble, it is reasonable

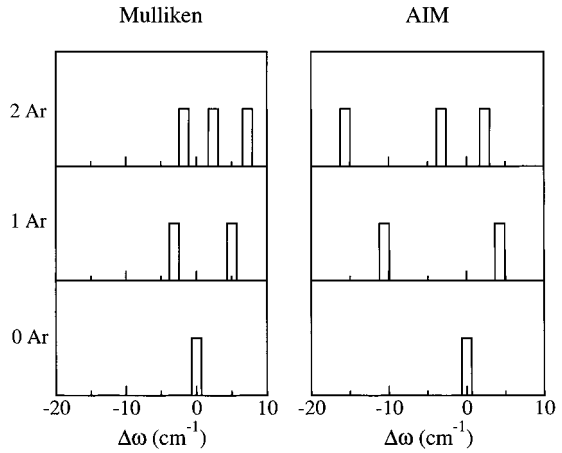

Figure 9. Calculated OH_{IHB} vibrational fundamentals for $Cl^-\cdot H_2O\cdot Ar_n$ ($n = 0, 1, 2$) using Mulliken and AIM point charges. $\Delta\omega$ represents the deviation of the calculated frequency from that of the OH_{IHB} in the unsolvated $Cl^-\cdot H_2O$ complex.

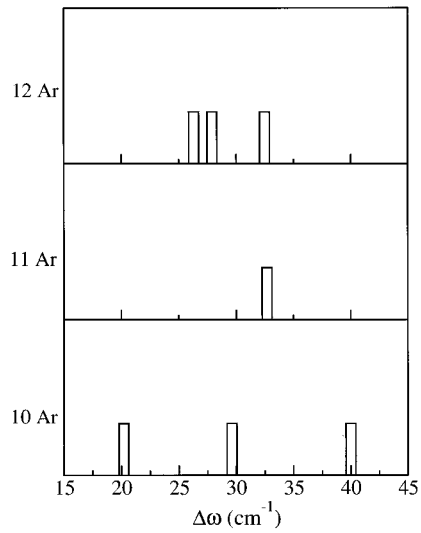

Figure 10. Calculated OH_{IHB} stretch spectrum for $Cl^-\cdot H_2O\cdot Ar_n$ ($n =$ 10, 11, and 12 Ar) using AIM point charges. $\Delta\omega$ represents the deviation of the calculated frequency from that of the OH_{IHB} in the unsolvated $Cl^-\cdot H_2O$ complex.

to expect some broadening about these calculated band origins, which would tend to blend together the two bands at higher energy. On the other hand, the $n = 2$ spectrum calculated using Mulliken charges does not reproduce the qualitative features of the experimental spectrum. The three peaks are calculated to fall in an interval of just 9.0 cm^{-1}, which would yield a narrower band than that displayed in the $n = 1$ spectrum with a shift to higher energy rather than the observed red shift. It can be concluded that, in the present application, Mulliken charges provide a poor description of the $Cl^-\cdot H_2O$ complex.

Figure 10 presents the calculated OH_{IHB} fundamentals (using AIM charges) for the $Cl^-\cdot H_2O\cdot Ar_n$ ($n = 10-12$) clusters. Once again, these patterns of band origins capture many of the qualitative features evident in the experimental spectra. Because a single isomer was obtained in our simulated annealing calculations on the $Cl^-\cdot H_2O\cdot Ar_{11}$ cluster, a single peak appears in the calculated spectrum, blue-shifted by 32.8 cm^{-1} relative to the band in unsolvated $Cl^-\cdot H_2O$. This calculation overestimates the blue shift of the $n = 11$ peak by 23 cm^{-1}. The calculations for $n = 10$ are consistent with the observed broad ($\sim$20 cm^{-1}) feature with possible multiplet structure, centered slightly below the $n = 11$ peak. The calculation for $n = 12$ predicts a new feature clearly red-shifted relative to the $n = 11$ peak and somewhat narrower than the $n = 10$ band envelope. This red-shift arises because the 12th argon atom is calculated to lie in the second solvation shell, close to the water molecule, whereas the clusters below $n = 11$ add additional argon atoms further from the water. In the experimental spectrum, this trend continues for $n = 13$, where we find a roughly additive shift similar to that displayed by the first two argon atoms, which again adopt positions close to the water molecule.

Given the obvious limitations of this one-dimensional electrostatic model, it nonetheless captures the qualitative spectral trends and even predicts the quantitative shifts much better than the previous methods.[29] In essence, our approach amounts to freezing the solvent in a particular arrangement and evaluating how this configuration affects the potential surface for motion of the hydrogen atom. Because of the high frequency of the hydrogen motion relative to that of the solvent, the shape of the surface is directly encoded in the level structure of this largely decoupled local oscillator. The presence of isomers then gives us a unique opportunity to explore how various "instantaneous" solvent configurations distort the surface in the entrance channel of the proton-transfer reaction eq 1. We can imagine these as snapshots of the dynamic local environment in a liquid, where the arrangement of argon atoms is constantly changing, leading to a time-dependent modulation of the vibrational level structure describing hydrogen motion.

From this perspective, clusters enable us to quantitatively establish the role of static solvation on the reaction coordinate. One important conclusion of this work is that the evolution of a high frequency oscillator embedded in a medium does not monotonically converge toward the bulk value established in a matrix-isolation experiment. In general, we expect the vibrational frequency to reflect two competing effects: a tendency to lower the frequency because of long range electrostatic stabilization of vibrationally excited states and a tendency to raise the frequency because of compression of the oscillator by the surrounding medium. It is clear, from the nonlinear frequency shifts exhibited in the experimental spectra and interpreted with our electrostatic solvation model, that the true situation is more complicated. Both red and blue shifts are generated by electrostatic effects alone.

It is, of course, an interesting and unresolved issue whether the isomers in the intermediate solvation regime, $Cl^-\cdot H_2O\cdot Ar_n$, $n = 3-10$, are themselves static or dynamic in character under our experimental conditions. Although not addressed in the present study, this issue can be explored by hole burning experiments in which part of the IHB band envelope is depleted while a second laser is scanned through the band. A dynamic cluster ensemble would be evident by hole filling in the isolated systems, and in such a scenario, picosecond time-resolved studies would be especially informative.

Another issue raised by our present analysis is whether our one-dimensional approach is valid for the description of the hydrogen motion in a finite medium. This issue can be challenged by measurement of the IHB locations for the OD oscillator as well as for overtone bands of the OH oscillator. Although the calculated OD fundamentals lie outside the range of our laser system, the $2 \leftarrow 0$ overtone of the OH stretch is calculated to be accessible using the intermediate frequency available in our OPO/OPA method of infrared generation. We have carried out preliminary experiments and found an absorption of the $Cl^-\cdot H_2O\cdot Ar$ complex at around 5919 cm^{-1}. This is surprisingly close to the calculated value for this transition (5917 cm^{-1}) when the calculated fundamental is scaled to the observed

value. Further experiments are underway to refine this measurement and search for higher vibrational levels.

Summary

The main result of this work is that the band envelope arising from excitation of the hydrogen bonded OH stretch in $Cl^-\cdot H_2O\cdot Ar_n$ clusters is selectively broadened upon argon solvation, displaying a minimum width at the same cluster size ($n = 11$) which displays a dramatic magic number in the parent ion intensity profile. Simulated annealing calculations indicate that the $n = 11$ cluster adopts a closed shell structure where the water molecule replaces an argon atom in the icosahedral $Cl^-\cdot Ar_{12}$ cluster. The evolution of the bandwidths can be understood with a model where the one-dimensional potential curve describing the motion of the hydrogen atom toward the chloride ion is electrostatically solvated by the argon atoms. Different isomers in the cluster ensemble then give rise to various shifts in the IHB bands, and the dominance of one isomeric form at $n = 11$ leads to a minimum in the width at this size.

Acknowledgment. We thank the National Science Foundation (CHE-0111245 and CHE-0075744) for support of this work. We also thank Professor Richard Saykally for the $Ar-H_2O$ potential and Professor Victor Batista for helpful discussions. M.A.J. also thanks Kevin Lisle for his valuable assistance in acquiring the spectra and W. H. Robertson for his help in the preliminary observation of the $2 \leftarrow 0$ overtone transition of the OH stretch.

References and Notes

(1) Ayotte, P.; Weddle, G. H.; Kim, J.; Johnson, M. A. *J. Am. Chem. Soc.* **1998**, *120*, 12361.
(2) Ayotte, P.; Kelley, J. A.; Nielsen, S. B.; Johnson, M. A. *Chem. Phys. Lett.* **2000**, *316*, 455.
(3) Bailey, C. G.; Kim, J.; Dessent, C. E. H.; Johnson, M. A. *Chem. Phys. Lett.* **1997**, *269*, 122.
(4) Ayotte, P.; Weddle, G. H.; Kim, J.; Johnson, M. A. *Chem. Phys.* **1998**, *239*, 485.
(5) Choi, J.-H.; Kuwata, K. T.; Cao, Y.-B.; Okumura, M. *J. Phys. Chem. A* **1998**, *102*, 503.
(6) Irle, S.; Bowman, J. M. *J. Chem. Phys.* **2000**, *113*, 8401.
(7) Combariza, J. E.; Kestner, N. R.; Jortner, J. *J. Chem. Phys.* **1994**, *100*, 2851.
(8) Dorsett, H. E.; Watts, R. O.; Xantheas, S. S. *J. Chem. Phys. A* **1999**, *103*, 3351.
(9) Zhan, C.-G.; Iwata, S. *Chem. Phys. Lett.* **1995**, *232*, 72.
(10) Kim, J.; Lee, H. M.; Suh, S. B.; Majumdar, D.; Kim, K. S. *J. Chem. Phys.* **2000**, *113*, 5259.
(11) Wright, N. J.; Gerber, R. B. *J. Chem. Phys.* **2000**, *112*, 2598.
(12) Zhao, X. G.; Gonzales-Lafont, A.; Truhlar, D. G.; Steckler, R. *J. Chem. Phys.* **1991**, *94*, 5544.
(13) Schenter, G. K.; Garrett, B. C. *J. Chem. Phys.* **2000**, *113*, 5171.
(14) Thompson, W. H.; Hynes, J. T. *J. Am. Chem. Soc.* **2000**, *122*, 6278.
(15) Tobias, D. J.; Jungwirth, P.; Parrinello, M. *J. Chem. Phys.* **2001**, *114*, 7036.
(16) Cabarcos, O. M.; Weinheimer, C. J.; Martinez, T. J.; Lisy, J. M. *J. Chem. Phys.* **1999**, *110*, 9516.
(17) Kelley, J. A.; Weber, J. M.; Lisle, K. M.; Robertson, W. H.; Ayotte, P.; Johnson, M. A. *Chem. Phys. Lett.* **2000**, *327*, 1−6.
(18) Robertson, W. H.; Kelley, J. A.; Johnson, M. A. *Rev. Sci. Instrum.* **2000**, *71*, 4431.
(19) Johnson, M. A.; Lineberger, W. C. In *Techniques for the Study of Gas-phase Ion Molecule Reactions*; Farrar, J. M., Saunders W. H., Eds.; Wiley: New York, 1988; Vol. 591.
(20) Arnold, S. T.; Hendricks, J. H.; Bowen, K. H. *J. Chem. Phys.* **1995**, *102*, 39.
(21) Becker, I.; Cheshnovsky, O. *J. Chem. Phys.* **1999**, *110*, 6288.
(22) Lenzer, T.; Yourshaw, I.; Furlanetto, M. R.; Pivonka, N. L.; Neumark, D. M. *J. Chem. Phys.* **2001**, *115*, 3578.
(23) Yourshaw, I.; Zhao, Y. X.; Neumark, D. M. *J. Chem. Phys.* **1996**, *105*, 351.
(24) Cohen, R. C.; Saykally, R. J. *J. Chem. Phys.* **1993**, *98*, 6007.
(25) Lenzer, T.; Yourshaw, I.; Furlanetto, M. R.; Reiser, G.; Neumark, D. M. *J. Chem. Phys.* **1999**, *110*, 9578.
(26) Aziz, R. A.; Slaman, M. J. *Mol. Phys.* **1986**, *58*, 679.
(27) Nielsen, S. B.; Ayotte, P.; Kelley, J. A.; Johnson, M. A. *J. Chem. Phys.* **1999**, *111*, 9593.
(28) Klots, C. E. *J. Chem.. Phys.* **1985**, *83*, 5854.
(29) Satoh, K.; Iwata, S. *Chem. Phys. Lett.* **1999**, *312*, 522.
(30) Dunning, T. H. *J. Chem. Phys.* **1989**, *90*, 1007.
(31) Kendall, R. A.; Dunning, T. H.; Harrison, R. J. *J. Chem. Phys.* **1992**, *96*, 6796.
(32) Xantheas, S. S. *J. Phys. Chem.* **1996**, *100*, 9703.
(33) Newell, A. C.; Baird, R. D. *J. Appl. Phys.* **1965**, *36*, 3751.
(34) Orcutt, R. H.; Cole, R. H. *J. Chem. Phys.* **1967**, *46*, 697.
(35) *Handbook of Chemistry and Physics*, 76th ed.; Lide, D. R., Jr., Ed.; CRC Press: Boca Raton, FL, 1995.
(36) Bader, R. F. W. *Atoms in Molecules: A Quantum Theory*; Oxford University Press: Oxford, U.K., 1990.